Development of innovative organic semiconductors driven by state-of-art analytical instruments

Toshihiro Okamoto*,**

1. Introduction to innovative molecular design technologies for organic electronics

Organic electronics based on organic semiconductors as an active layer have been extensively researched as next-generation electronic devices. To develop the market for organic electronic devices such as integration circuits and sensors, the carrier mobility (hereinafter referred to as the mobility) is an important parameter for device performance and needs to be improved significantly (Fig. 1). Additionally, considering applicable organic electronics, organic semiconductors must exhibit the following features: 1) chemical and thermal stabilities during the device fabrication process and in the operating environment, 2) device durability under ambient air and bias stress, and 3) solution-processability. To achieve these requirements, innovations in molecular design technologies are needed.

A representative organic semiconducting π-electron core (π-core) is pentacene, which consists of linearly-fused five benzene rings and is classified as an acene. Pentacene aggregates through multiple intermolecular C–H···π interactions to form a two-dimensional herringbone-type packing structure, which is suitable for carrier transport. This structure results in a mobility higher than that of currently used amorphous silicon (0.5–1.0 cm^2/Vs)[1]. However, pentacene gradually decomposes under ambient air to give oxidized pentacenes such as 6,13-pentacene quinone[2], which makes it difficult to use under ambient conditions.

One molecular design strategy to improve its chemical stability is to replace the highly reactive central benzene ring containing 6- and 13-position-carbons with heterole rings to produce [1]benzothieno-[3,2-*b*][1]benzothiophene (BTBT) or dinaphtho[2,3-*b*:2′,3′-*f*]thieno[3,2-*b*]thiophene (DNTT) (Fig. 2)[3, 4]. DNTT forms herrigbone-type packing, similar to the case with pentacene, and shows a higher mobility under ambient conditions[4].

Although the π-cores of DNTT and BTBT are chemically stable, they have a poor solubility in common organic solvents. Hence, they cannot be prepared via solution processes[5]. One molecular design strategy to improve the solubility is to introduce flexible long alkyl[3, 6, 7] or bulky substituents[8] into the cores. This strategy not only enhances the solubility but also contributes to molecular self-aggregation due to the intermolecular van der Waals interactions between substituents to achieve a higher mobility than non-substituted ones[3,6,7].

Pentacene, DNTT, and BTBT, are categorized as linear or quasilinear π-cores. They tend to exhibit molecular motions such as rotation and translation around the long and short molecular axes, respectively (Fig. 3). Introducing flexible alkyl chains induces a phase transition from the initial crystal phase into either the liquid crystal phase or the fluid phase by external stimuli such as heat. Actually, decyl-substituted pentacene (C10-Pen), BTBT (C10-BTBT), and DNTT (C10-DNTT) show lower phase transition temperatures of 89 °C, 109 °C, and 117 °C, respectively[3, 9, 10]. Furthermore, thin-film transistors based on C10-BTBT and C10-DNTT are not driven more than these phase transition temperatures. Recently, asymmetrically substituted BTBT with decyl and phenyl groups (C10-BTBT-Ph) was developed. It shows a high-ordered liquid crystal (SmE) phase, leading to a higher phase transition temperature around 150 °C[13].

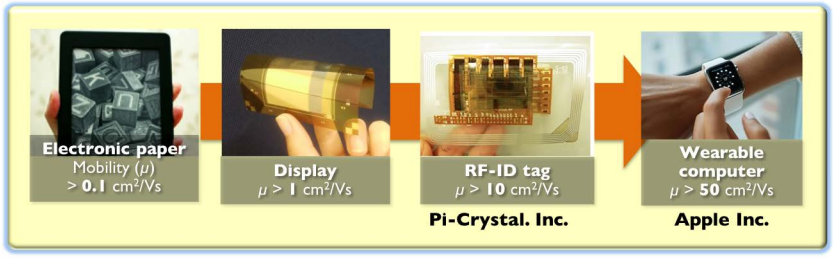

Fig. 1. Relationship between the carrier mobility and practical applications based on organic electronics.

* Department of Advanced Materials Science, Graduate School of Frontier Sciences, The University of Tokyo.
** PRESTO, JST

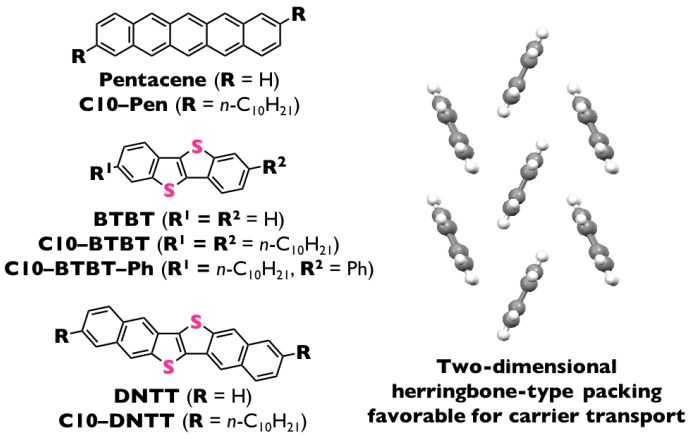

Fig. 2. Representative organic semiconducting molecules and two-dimensional herringbone-type packing structure favorable for carrier transport.

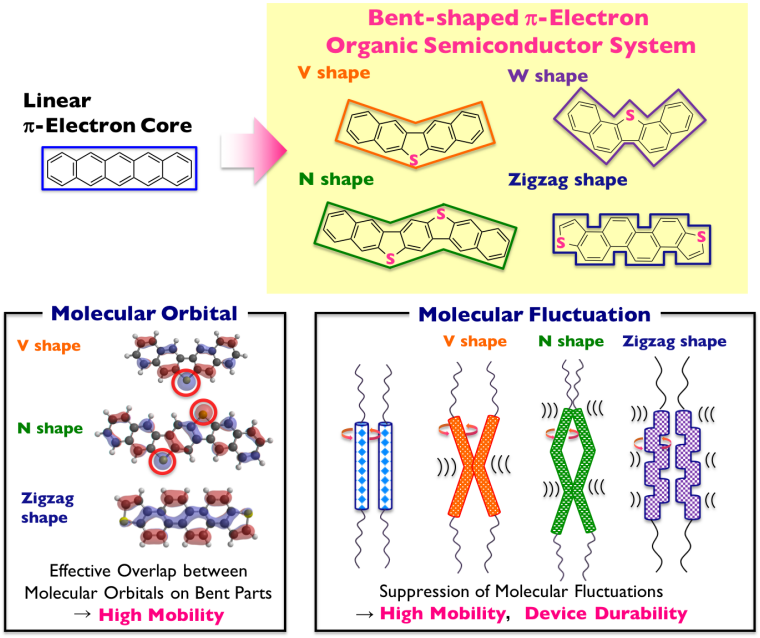

Fig. 3. Molecular design strategy for first- and the second-generation "bent-shaped organic semiconductors".

To develop organic semiconductors for practical applications, both the material stability and device durability during device fabrication processes (e.g., wiring and electrode patterning, which is generally 150–200 °C)[14] and the usage environment (e.g., in-car applications) must be enhanced. Our group has developed conceptually new organic semiconductors by means of both chemical and device engineering approaches. Organic semiconductors based on bent-shaped π-electron cores[15]–[28] (Fig. 3) are promising molecular systems that exhibit the aforementioned required features. Herein our strategic development scheme for a high-performance organic semiconductor molecular system, which takes advantage of state-of-the-art analytical instruments, is described.

2. Strategic development scheme for a high-performance organic semiconductor molecular system

2.1. Molecular design strategy for a semiconducting molecular system

The reported molecular design for organic semiconductors is based on linear- or quasilinear-shaped π-cores composed of highly fused acenes and heteroacenes (Fig. 2). We have demonstrated new π-cores conceptually as a unique and innovative molecular design strategy that focuses on molecular shape and charge transport based on "bent"-shaped π-cores (Fig. 3). Element-bridged V-shaped π-cores are the first generation of bent-shaped π-cores.

The molecular design strategy for V-shaped π-cores is as follows. Regarding the mobility, effective intermolecular orbital overlap between the central

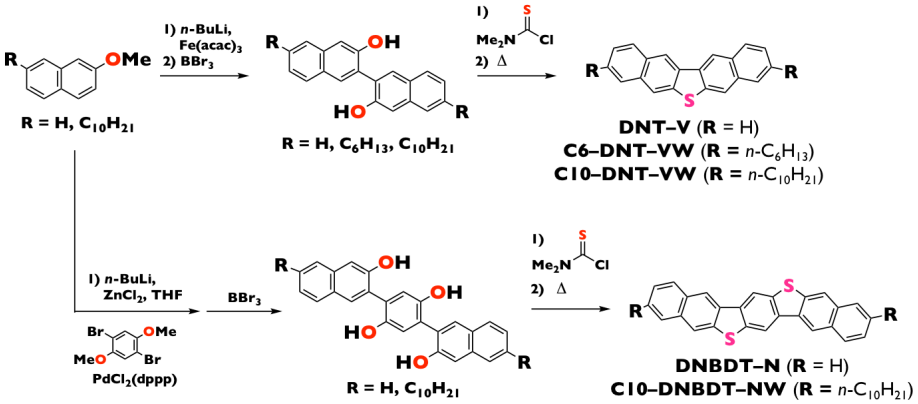

Scheme 1. Synthesis for V-shaped and N-shaped derivatives.

prominent sulfur atoms with a large orbital coefficient in the highest occupied molecular orbital (HOMO) as well as suppressed molecular fluctuations along the long axis (intermolecular fluctuations mainly degrade the carrier transport) by the V-shaped feature may realize a high carrier mobility. In addition, suppressing intermolecular fluctuations should contribute to thermal stability of the aggregated form, leading to a high thermal device durability. Furthermore, the bent π-core system is scientifically attractive because sulfur at the bent position can easily be replaced with other elements using reported synthetic methodologies to input the desired properties. To improve the intermolecular orbital overlap among molecules and to suppress the intermolecular fluctuations, π-extended V-shaped molecules, namely N-shaped π-cores with two bent parts, have been developed.

Very recently, the second-generation bent-shaped π-cores have been realized by focusing on the "molecular orbital configuration". In addition to the molecular design strategy for the first generation, second-generation bent π-cores have a small change rate of the transfer integrals along the molecular long axis. So, the intermolecular fluctuations in the second-generation bent π-cores are less effective while the molecules fluctuate in the lamellar-aggregated structure (e.g., herringbone-type packing structure)[27]. Hereinafter, details about the first-generation π-cores, V-shaped and N-shaped molecules, are explained.

2.2. Synthesis of V-shaped and N-shaped molecules

V-shaped derivatives, DNT-V, C6-DNT-VW, and C10-DNT-VW, are easily synthesized in high yields by oxidative homo coupling[29], demethylation, and annulation reaction via a Newman–Kwart rearrangement[30] (Scheme 1). The synthesis is reproducible even on the gram scale without an expensive catalyst such as palladium, suggesting a high practical applicability. The synthesis of N-shaped derivatives, DNBDT-N and C10-DNBDT-NW, can be applied via the same key reactions as V-shaped cases.

2.3. Solubility test

Organic semiconductors can be prepared via solution processes, which are critical to realize a low-cost device fabrication. The solubility of V-shaped and N-shaped derivatives, DNT-V, C6-DNT-VW, C10-DNBDT-NW, were investigated in toluene at room temperature or 60 °C. Notably, unsubstituted DNT-V exhibits a solubility of 0.17 wt%. Under the same conditions, the solubilities of unsubstituted pentacene and DNTT are at least two magnitudes smaller. Introducing flexible alkyl substituents into DNT-V, C6-DNT-VW shows a much higher solubility (approximately 1.0 wt%). Consequently, various solution processes, including spin-coating, inkjet-printing, and drop-casting, can be applied to this derivative. Moreover, the alkyl-substituted N-shaped derivative, C10-DNBDT-NW, which has seven fused aromatic rings, shows at least a one order of magnitude higher solubility (ca. 0.03 wt% in toluene at 60 °C) than the same alkyl-substituted DNTT with six fused aromatic rings under the same conditions. In contrast, C10-DNBDT-NW is less soluble than the V-shaped analog due to its highly π-extended core.

2.4. Evaluation of chemical and thermal stabilities

To evaluate the chemical stability in the molecular and aggregated forms, the time-dependent UV-vis spectra were continuously measured for two weeks in solution and evaporated thin films (100-nm thick), respectively. Although all the derivatives are stocked under ambient air, their spectra do not change over time, indicating that derivatives based on V- and N-shaped π-cores are chemically stable in both forms. Hence, they can be handled in ambient air without special care.

Next, simultaneous measurements of thermogravimetry (TG) and differential thermal analysis (DTA), the so-called TG-DTA, were performed to investigate their thermal stabilities. TG-DTA measurements provide information about the exothermic and endothermic changes due to thermal decomposition, phase transition, etc. as well as weight changes due to sublimation, evaporation, etc. TG-DTA measurements under nitrogen

gas flow reveal that a series of V-shaped and N-shaped derivatives melt and subsequently evaporate or sublime without decomposition. Hence, they are thermally stable. Furthermore, the phase transition temperatures from the initial crystal phase are 150 °C, 200 °C, and 216 °C for C10-DNT-VW, C6-DNT-VW, and C10-DNBDT-NW, respectively. These values are much higher than those of C10-Pen (89 °C)[9], C10-BTBT (109 °C)[3], and C10-DNTT (117 °C)[10] described above. These findings suggest that bent-shaped π-cores more effectively interact to suppress molecular motions. Their highly stabilized crystal phase is important for organic semiconductor applications.

2.5. Purification and purity evaluation

Since organic semiconductors are used as active layers in electronic devices, their purity significantly impacts device performance such as life-time, reliability, and reproducibility. As described in Section 2.4, all of the derivatives are chemically and thermally stable. Numerous techniques can be used to purify the derivatives, including column chromatography, recrystallization, sublimation, etc. Prior to the purification process, information about their solubility or the 5% weight loss temperature was used as a reference.

The degree of purity was estimated by gas chromatography (GC) and/or high performance liquid chromatography (HPLC). Since V-shaped derivatives have a sufficient solubility in common polar organic solvents (e.g., tetrahydrofuran and acetonitrile), their purities are easily determined. On the other hand, the N-shaped derivative, C10-DNBDT-NW, exhibits a poor solubility in certain solvents, making purity evaluations difficult via the same method. Hence, sampling conditions as well as equipment and facilities need to be optimized. A LC-MS machine equipped with a highly sensitive detector is a powerful tool to evaluate purity accurately. Using a combination of LC-MS and optimized conditions, the target material and impurities were successfully detected. The high-sensitivity detector allows samples at a low concentration to be measured.

2.6. Crystal growth and single crystal structural analysis

To understand and forecast the potential of organic semiconductors, their aggregation structures must be clarified by X-ray single crystal structural analysis. Using structural information, the transfer integral and effective mass were calculated theoretically to forecast the carrier transport capability prior to evaluating actual transistors.

First, single crystals of C10-DNT-VW and C10-DNBDT-NW were grown by solution techniques such as the bilayer diffusion method or the vapor diffusion method using a good solvent and a poor solvent, or crystallization under temperature ramping due to the sufficient solubility of both compounds. On the other hand, unsubstituted DNT-V and DNBDT-N, which have poor solubilities, were grown via a physical vapor transport technique (PVT)[31]. In terms of the single crystals grown by solution techniques, drying on a filter paper is crucial prior to X-ray single crystal structural analysis as it improves the crystallinity and allows Laue spots at higher angles to be detected (Fig. 4). Since almost all of compounds form small and thin platelet single crystals, an imaging plate (IP) equipped with a high dynamic range and hybrid photon counting (HPC) was employed as a detector to endure the long-time X-ray exposure.

Figures 5a and 5b illustrate the molecular and packing structures of C10-DNT-VW in a single crystal. The molecular structure exhibits a distorted conformation,

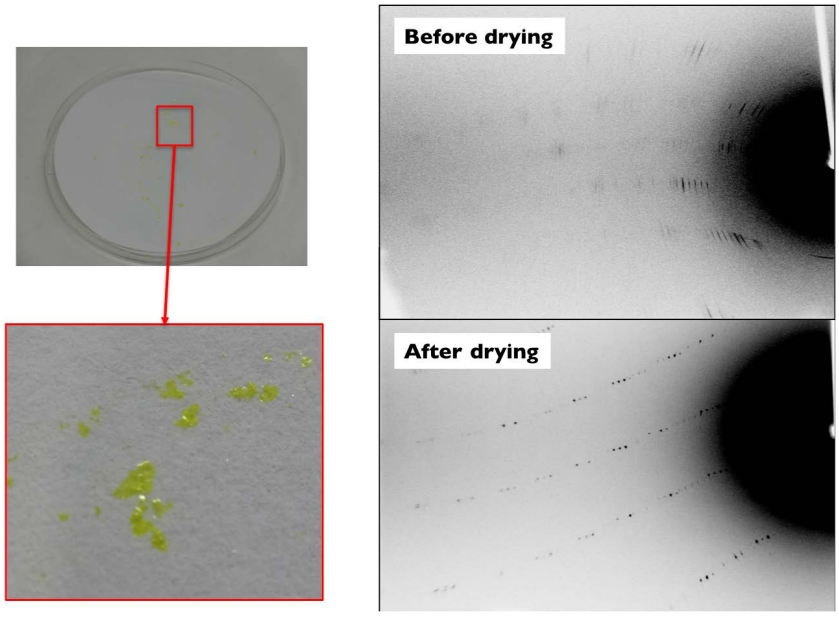

Fig. 4. (Right) Example of the difference upon drying crystals and (left) the change in the XRD pattern of C10-DNT-VW upon drying.

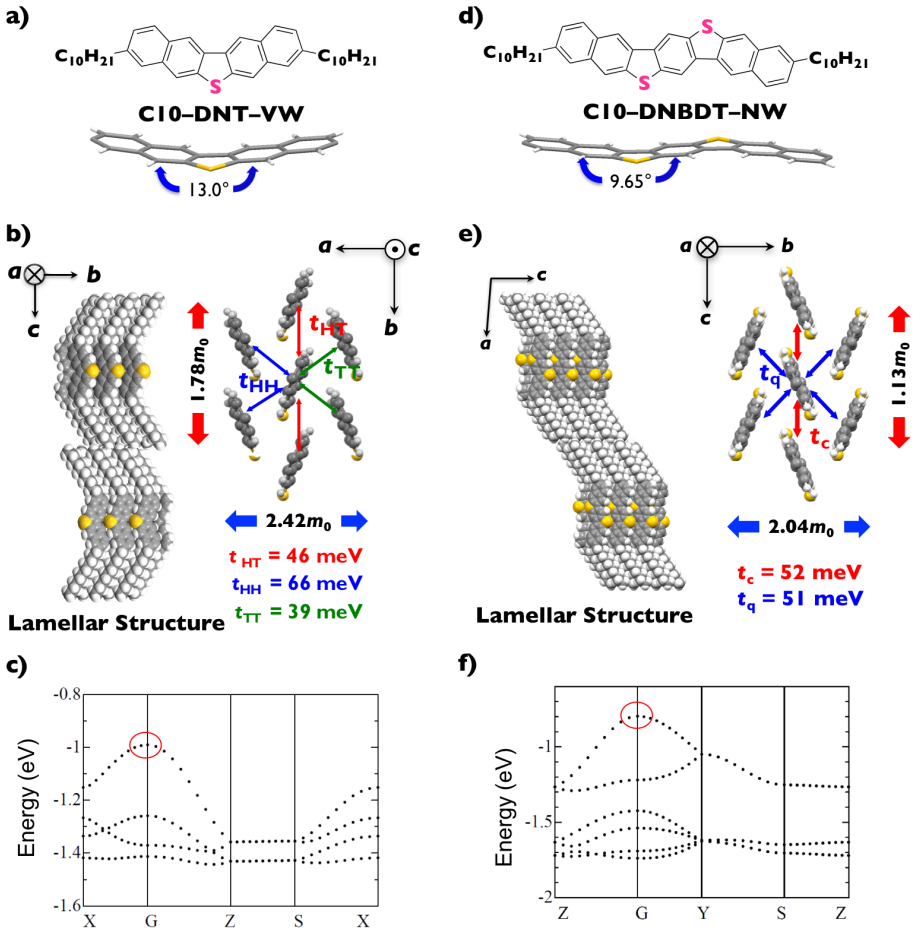

Fig. 5. a) Chemical and molecular structures in a crystal, b) packing structure with transfer integrals and effective masses, and c) the band structure of C10-DNT-VW. d) Chemical and molecular structures in a crystal, e) packing structure with transfer integrals and effective masses, and f) the band structure of C10-DNBDT-NW.

unlike the planar one optimized by DFT calculations. The packing composes a lamellar structure along the *c* axis and a two-dimensional herringbone structure in the *a*–*b* plane. These are favorable for carrier transport and have been observed in the case of high-mobility organic semiconductors such as pentacene and DNTT. Unsubstituted and other alkyl-substituted DNT-Vs also exhibit the same herringbone packing structure.

Based on the crystal structures obtained in X-ray single crystal analyses, the transfer integrals were estimated at the PBEPBE/6-31G(d) level. The transfer integral reflects the molecular orbital overlaps between neighboring molecules. Thus, it is an important parameter to describe carrier transport phenomena. Among the seven molecules in the *a*–*b* plane, each transfer integral between two neighboring molecules was calculated. Unsubstituted DNT-V exhibits transfer integrals of 41, 50, and 18 meV. The transfer integral that is lower than the others is partly due to the intermolecular displacement along the *c*-axis (molecular long axis). On the other hand, in C10-DNT-VW, the lack of intermolecular displacement along the same axis and the smaller distance between centroids lead to larger transfer integrals of 46, 66, and 39 meV for all directions. Therefore, C10-DNT-VW should show a higher mobility than unsubstituted DNT-V. The N-shaped derivative, C10-DNBDT-NW, exhibits a distorted molecular structure at the two thiophene rings, a lamellar structure in the direction of the long molecular axis, and a two-dimensional herringbone-type packing structure in the layer (Figs. 5d, e). Its transfer integrals are large with values greater than 50 meV in all directions.

Furthermore, the band structures were also calculated at the same PBEPBE/6-31G(d) level as the transfer integrals. The band structures provide the effective mass, which indicates the ostensible weight of a carrier and a smaller value in the more conductive direction. Figures 5c and 5f plot the band structures of C10-DNT-VW and C10-DNBDT-NW where the horizonal axis indicates the line connecting the points of X=(0.5, 0,0), Γ=(0, 0, 0), Y=(0, 0.5, 0), S=(0.5, 0.5, 0), and X=(0.5, 0, 0) in the first Brillouin zone. The effective masses at the Γ point, which is the band with the maximum curvature, were employed. The aggregated structure of C10-DNBDT-NW has effective masses of 1.13 m_0 and 2.04 m_0 in the column direction and the transverse direction, respectively (m_0

is the weight of carrier in vacuum). These values and the anisotropy are smaller than those of C10-DNT-VW ($1.78\,m_0$ and $2.42\,m_0$). Thus, aggregated structures and theoretical calculations based on structural information are extremely useful to screen promising organic semiconductors.

2.7. Structural analysis, surface morphology, and ionization potential of thin films

Since the structure, surface morphology, and ionization potential in thin film impact the evaluation of a semiconductor, X-ray diffraction (XRD), atomic force microscopy (AFM), and photoelectron yield spectroscopy (PYS) were performed. XRD provides information about the aggregated structure in thin film. In the case of a polycrystalline organic semiconductor thin film, the out-of-plane diffraction is mainly measured because many small crystals randomly assemble, which provides less information about the in-plane structure. On the other hand, for single crystalline thin films, both in-plane and out-of-plane diffraction patterns clearly exhibit proper directions for carrier transport along the channel length. AFM images provide information about morphology; the cracks prevent conduction in a single crystal and flatness of the surface. In the case of polycrystalline films, the surface morphology such as the grain size by AFM observations is an indicator of conduction in the film. The ionization potential of organic thin films determined by PYS is an indicator of the carrier injection barriers between metal electrodes and organic semiconductors in which Fermi pinning hardly occurs.

Initially a single crystalline film was prepared for each of the derivatives. For unsubstituted derivatives with a poor solubility, single crystals grown by a PVT technique were laminated onto substrates[32]. For soluble C10-DNT-VW and C10-DNBDT-NW, their crystalline films were constructed by an edge casting technique[33] (Fig. 6a). For these single crystalline thin-films, structural analyses, morphological observations, and evaluations of the ionization potentials were performed. Figures 6b and 6e show the X-ray diffraction pattern and an AFM image of the C10-DNBDT-NW single crystalline thin-film. The Laue spots in the XRD pattern could be assigned assuming that the crystalline film and the single crystal for X-ray single crystal structural analysis have the same structure. The results indicate that the molecular long axis and the direction with a small effective mass are almost perpendicular to the substrate and along the direction of crystal growth, respectively. According to the results, a channel should be constructed along the direction with a small effective mass. This allows new organic semiconductors to be effectively evaluated. AFM observations of various places do not detect cracks except those observed by a microscope, which suggesting that the film is a high-quality crystalline film.

PYS reveals that the ionization potentials of DNT-V, C10-DNT-VW, and C10-DNBDT-NW are 5.72, 5.46, and 5.24 eV, respectively. These values are slightly larger than the work function of the Au electrode (~5.0 eV), indicating that the materials work as p-type organic semiconductors. Additionally, holes are most easily injected into C10-DNBDT-NW.

2.8. Transistor fabrication and evaluation of semiconductor performance with FETs

The transistor structures were fabricated as 2,3,5,6-tetrafluoro-7,7,8,8-tetracyanoquinodimethane (F4-TCNQ, 2 nm) and gold (50 nm) was deposited through a metal mask onto a crystalline film constructed as mentioned above on a SiO_2/dope Si wafer (Figs. 7a, b). To improve the wettability for an organic solution, the surface of the wafer used in the edge casting technique was treated with self-assembled monolayers (SAMs), β-phenyltriethoxysilane (β-PTS), in advance. F4-TCNQ is an electron-accepting molecule, and its layer between organic semiconductors and electrodes reduces the contact resistance. The fundamental characteristics of the OFETs were obtained as the drain current I_D, which was measured under a gate voltage V_G and a drain voltage V_D using a source meter or a semiconductor parameter analyzer equipped with source measure units (SMUs). The mobility in the saturation region, μ_{sat}, was calculated using the formula based on a gradual channel approximation, $I_D = (1/2)\cdot\mu_{sat}\cdot C\cdot(W/L)\cdot(V_G - V_{th})^2$, where C is the capacitance of the gate insulator, and L and W are the length and width of the channel, respectively.

As typical characteristics of OFETs based on obtained crystalline films, Figs. 7c and 7d show the transfer and output characteristics of an OFET based on the C10-DNBDT-NW solution-processed crystalline film. As expected from the ionization potentials, all OFETs based on V-shaped and N-shaped derivatives operate as p-type OFETs in which I_D increases when applying a negative

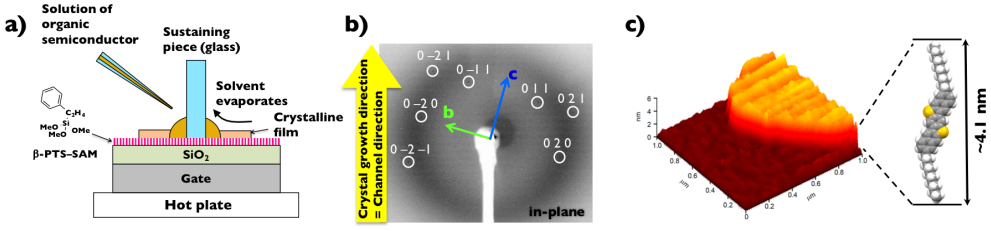

Fig. 6. a) Illustration of the edge casting method. b) Transparent X-ray diffraction pattern and c) AFM image of a C10-DNBDT-NW solution-processed crystalline film.

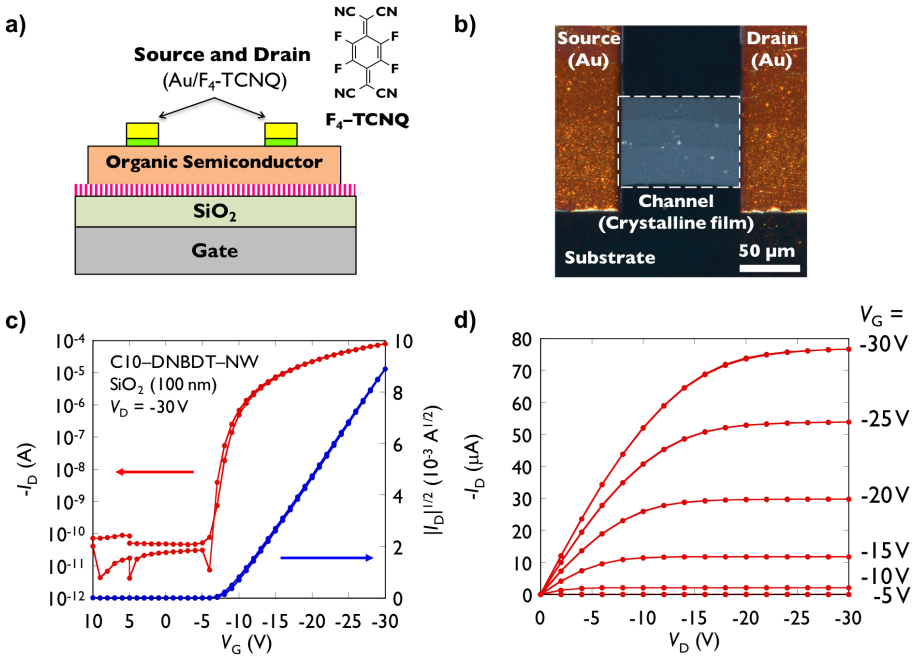

Fig. 7. a) Bottom-gate top-contact OFET. b) Polarization microscopic image, c) transfer and d) output characteristics of an OFET of a C10-DNBDT-NW crystalline film.

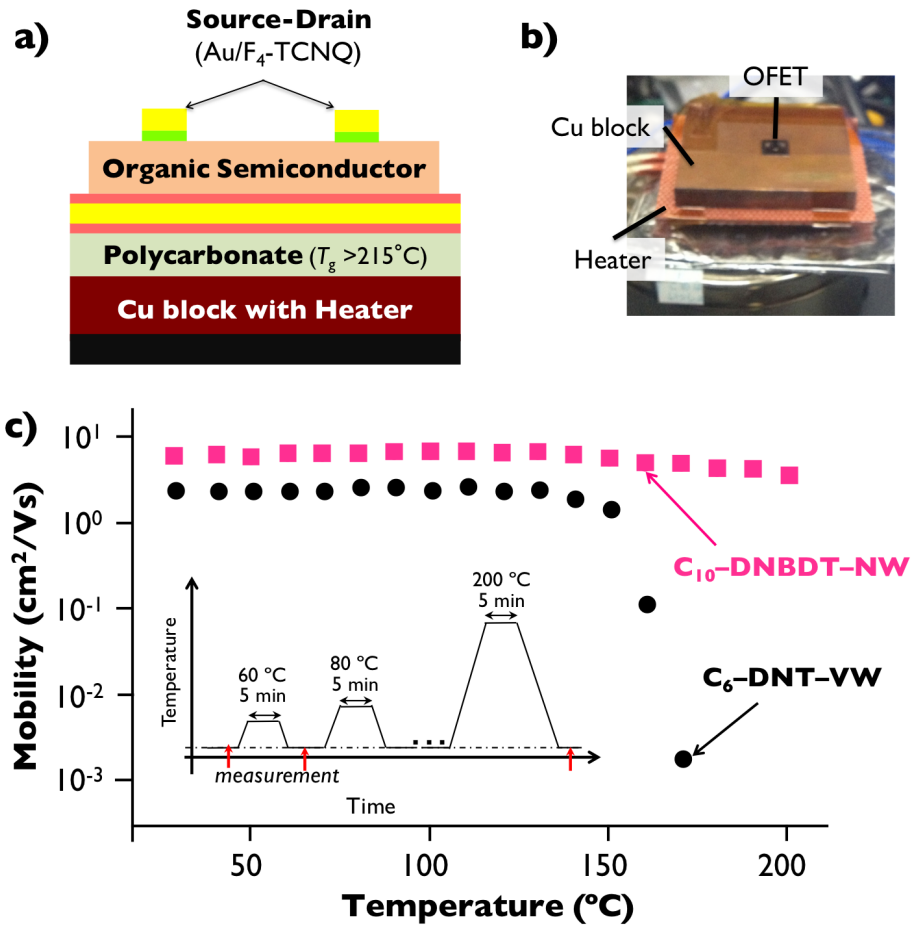

Fig. 8. Thermal stress test for OFETs based on C6-DNT-VW and C10-DNBDT-NW. a) Device structure for a thermal stress test, b) picture of the actual set up, and c) temperature dependence of the mobility. (inset) Schematic procedure for the thermal stress test.

V_G. Their output characteristics show saturation of I_D, indicating textbook-like OFET operations. The values of μ_{sat} agree well with the theoretically calculated transfer integrals and effective masses; the values increase in the order of DNT-V, C10-DNT-VW, and C10-DNBDT-NW. Among the obtained V-shaped and N-shaped materials, C6-DNT-VW and C10-DNBDT-NW show the highest mobility ($>10\,cm^2/Vs$).

For OFETs based on high mobility C6-DNT-VW and C10-DNBDT-NW crystalline films, thermal stress tests were performed (Fig. 8). For the heating tests, polycarbonate substrates with thermal shrinkages comparable to organic semiconductors were employed. These transistor performances were measured at room temperature after heating at each temperature for 5 minutes and cooling to room temperature. Transistors based on C6-DNT-VW do not show a remarkable mobility degradation up to 150 ℃. The mobility degradation at temperatures lower than the liquid crystal transition temperature of C6-DNT-VW (200ºC) is due to sublimation of the molecules even at ambient pressure, which was observed by microscopy. In contrast, C10-DNBDT-NW with a larger molecular weight and a stronger intermolecular interaction is thermally stable up to 200 ℃ in devices. Furthermore, storage tests and bias stress tests were also performed. The mobility of these OFETs does not remarkably degrade. Thus, organic semiconductors of C6-DNT-VW and C10-DNBDT-NW are stable against stress in the operating environment.

3. Conclusion and perspective

Herein recent works on high-performance organic semiconductors in organic transistors are reviewed. To develop new organic semiconductors promptly and effectively, basic scientific technologies such as analysis and measurement techniques are indispensable. To accelerate future developments of practical organic semiconductor applications, innovation of such new instruments should be linked with material development. A goal for the near-future is that flexible wearable devices based on organic semiconductors are used in practical situations.

Acknowledgement

This work was supported by the JST PRESTO program “Molecular Technology and Creation of New Functions” (supervised by Prof. Takashi Kato, project code: JPMJPR13K5 and JPMJPR17R2) and KAKENHI. T.O. thanks JSPS for Grants-in-Aid for Scientific Research (B; No. 25288091, 17H03104).

References

(1) Y.-Y. Lin, D. J. Gundlach, S. F. Nelson and T. N. Jackson: *IEEE Electron Device Letters*, **18** (1997), 606−608.
(2) A. Maliakal, K. Raghavachari, H. Katz, E. Chandross and T. Siegrist: *Chem. Mater.*, **16** (2004), 4980−4986.
(3) H. Ebata, T. Izawa, E. Miyazaki, K. Takimiya, M. Ikeda, H. Kuwabara and T. Yui: *J. Am. Chem. Soc.*, **129** (2007), 15732−15733.
(4) T. Yamamoto and K. Takimiya: *J. Am. Chem. Soc.*, **129** (2007), 2224−2225.
(5) Y. Natsume, T. Minakata and T. Aoyagi: *Org. Electron.*, **10** (2009), 107−114.
(6) M. J. Kang, I. Doi, H. Mori, E. Miyazaki, K. Takimiya, M. Ikeda and H. Kuwabara: *Adv. Mater*., **23** (2011), 1222−1225.
(7) K. Nakayama, Y. Hirose, J. Soeda, M. Yoshizumi, T. Uemura, M. Uno, W. Li, M. J. Kang, M. Yamagishi, Y. Okada, E. Miyazaki, Y. Nakazawa, A. Nakao, K. Takimiya and J. Takeya: *Adv. Mater.*, **23** (2011), 1626−1629.
(8) J. E. Anthony, J. S. Brooks, D. L. Eaton and S. R. Parkin: *J. Am. Chem. Soc.*, **123** (2001), 9482−9483.
(9) K. Okamoto, T. Kawamura, M. Sone and K. Ogino: *Liq. Cryst.*, **34** (2007), 1001−1007.
(10) H. Kuwabara, M. Ikeda and K. Takimiya: (2010), WO 2010/098372 A1.
(11) H. Iino, T. Kobori and J. Hanna: *J. Non-Cryst. Solids*, **358** (2012), 2516−2519.
(12) T. Yokota, K. Kuribara, T. Tokuhara, U Zschieschang, H. Klauk, K. Takimiya, Y. Sadamitsu, M. Hamada, T. Sekitani and T. Someya: *Adv. Mater.*, **25** (2013), 3639−3644.
(13) H. Iino, T. Usui and J. Hanna: *Nat. Commun.*, **6** (2015), 6828.
(14) K. Kuribara, H. Wang, N. Uchiyama, K. Fukuda, T. Yokota, U. Zschieschang, C. Jaye, D. Fischer, H. Klauk, T. Yamamoto, K. Takimiya, M. Ikeda, H. Kuwabara, T. Sekitani, Y.-Lin Loo and T. Someya: *Nat. Commun.*, **3** (2012), 723.
(15) T. Okamoto, C. Mitsui, M. Yamagishi, K. Nakahara, J. Soeda, Y. Hirose, K. Miwa, H. Sato, A. Yamano, T. Matsushita, T. Uemura and J. Takeya: *Adv. Mater*., **25** (2013), 6392−6397.
(16) C. Mitsui, T. Okamoto, H. Matsui, M. Yamagishi, T. Matsushita, J. Soeda, K. Miwa, H. Sato, A. Yamano, T. Uemura and J. Takeya: *Chem. Mater.*, **25** (2013), 3952−3956.
(17) K. Nakahara, C. Mitsui, T. Okamoto, M. Yamagishi, K. Miwa, H. Sato, A. Yamano, T. Uemura and J. Takeya: *Chem. Lett.*, **42** (2013), 654−656.
(18) K. Nakahara, C. Mitsui, T. Okamoto, M. Yamagishi, J. Soeda, K. Miwa, H. Sato, A. Yamano, T. Uemura and J. Takeya: *Jpn. J. Appl. Phys.*, **52** (2013), 05DC10.
(19) K. Nakahara, C. Mitsui, T. Okamoto, M. Yamagishi, H. Matsui, T. Ueno, Y. Tanaka, M. Yano, T. Matsushita, J. Soeda, Y. Hirose, H. Sato, A. Yamano and J. Takeya: *Chem. Commun.*, **50** (2014), 5342−5344.
(20) C. Mitsui, Y. Tanaka, S. Tanaka, M. Yamagishi, K. Nakahara, M. Yano, H. Sato, A. Yamano, H. Matsui, J. Takeya and T. Okamoto: *RSC Adv.*, **6** (2016), 28966−28969.
(21) C. Mitsui, H. Tsuyama, R. Shikata, Y. Murata, H. Kuniyasu, M. Yamagishi, H. Ishii, A. Yamamoto, Y. Hirose, M. Yano, T. Takehara, T. Suzuki, H. Sato, A. Yamano, E. Fukuzaki, T. Watanabe, Y. Usami, J. Takeya and T. Okamoto: *J. Mater. Chem. C*, **5** (2017), 1903−1909.
(22) C. Mitsui, T. Annaka, K. Nakamura, M. Mitani, D. Hashizume, K. Nakahara, M. Yamagishi, T. Ueno, Y. Tanaka, M. Yano, D. Iwasawa, M. Hasegawa, H. Sato, A. Yamano, J. Takeya and T. Okamoto: *Polym. J.*, **49** (2017), 215−221.
(23) T. Kubo, R. Häusermann, J. Tsurumi, J. Soeda, Y. Okada, Y. Yamashita, N. Akamatsu, A. Shishido, C. Mitsui, T. Okamoto, S. Yanagisawa, H. Matsui and J. Takeya: *Nature Commun.*, **7** (2016), 11156.
(24) C. Mitsui, M. Yamagishi, R. Shikata, H. Ishii, T. Matsushita, K. Nakahara, M. Yano, H. Sato, A. Yamano, J. Takeya and T. Okamoto: *Bull. Chem. Soc. Jpn*., **90** (2017), 931−938.
(25) I. Piquero-Zulaica, J. Lobo-Checa, A. Sadeghi, Z. M. A. El-Fattah, C. Mitsui, T. Okamoto, R. Pawlak, T. Meier, A. Arnau, J E. Ortega, J. Takeya, S. Goedecker, E. Meyer and S Kawai: *Nature Commun.*, **8** (2017), 787.
(26) J. Tsurumi, H. Matsui, T. Kubo, R. Häusermann, C. Mitsui, T. Okamoto, S. Watanabe and J. Takeya: *Nat. Phys.*, **13** (2017), 994−998.
(27) A. Yamamoto, Y. Murata, C. Mitsui, H Ishii, M. Yamagishi, M. Yano, H. Sato, A. Yamano, J. Takeya and T. Okamoto: *Adv. Sci*., **5** (2018), 1700317.
(28) A. Yamamura, S. Watanabe, M. Uno, M. Mitani, C. Mitsui, J.

Tsurumi, N. Isahaya, Y. Kanaoka, T. Okamoto and J. Takeya: *Sci. Adv.*, **4** (2018), eaao5758.
(29) M. J. Marsella, P. J. Carroll and T. M. Swager: *J. Am. Chem. Soc.*, **116** (1994), 9347−9348.
(30) G. C. Lloyd-Jones, J. D. Moseley and J. S. Renny: *Synthesis*, **5** (2008), 661−689.
(31) Ch. Kloc, P. G. Simpkins, T. Siegrist and R. A. Laudise: *J. Cryst. Growth*, **182** (1997), 416−427.
(32) J. Takeya, C. Goldmann, S. Haas, K. P. Pernstich, B. Ketterer and B. Batlogg: *J. Appl. Phys*., **94** (2003), 5800−5804.
(33) T. Uemura, Y. Hirose, M. Uno, K. Takimiya and J. Takeya: *Appl. Phys. Express*, **2** (2009), 111501.